



HFF  
17,4

418

Received 4 November 2004  
Revised 14 July 2006  
Accepted 14 July 2006

# Numerical simulation of time-dependent heat and fluid flows inside and around single rising bubbles using a moving axisymmetric boundary-fitted mesh system

Huanxin Lai

*School of Mechanical and Power Engineering,  
East China University of Science and Technology, Shanghai,  
People's Republic of China and*

*Thermofluids and Superconductivity Group, School of Engineering Sciences,  
University of Southampton, Southampton, UK*

Yuying Yan

*School of Built Environment, University of Nottingham,  
Nottingham, UK, and*

Keqi Wu

*School of Energy and Power Engineering,  
Huazhong University of Science and Technology, Wuhan,  
People's Republic of China*

## Abstract

**Purpose** – This paper aims to develop a numerical method for analysing the time-dependent conjugate heat and fluid flows inside and around single bubbles rising in a hot liquid.

**Design/methodology/approach** – The procedure combines the moving mesh method for flows in time-dependent geometries and the zoned calculation algorithm for conjugate viscous flows. A moving axisymmetric boundary-fitted mesh is used to track the deformable gas-liquid interface, while conjugate flows in both gas and liquid sides are calculated by a two-block zoned method. The interfacial stresses are employed to calculate the velocity value and to decide the time-dependent bubble shape simultaneously. Governing equations for the rising velocity and acceleration of the bubble are derived according to the forces acting on the bubble.

**Findings** – A calculating procedure for time-dependent conjugate heat and fluid flows inside and around a rising single bubble has been developed. The algorithm has been verified, and can be employed for further analysing heat, mass and momentum transfer phenomena and their relevant mechanisms.

**Originality/value** – The paper developed a method to obtain high fidelity results for the heat and fluid flow details in the vicinity of a time-dependent moderately deformable rising bubble; the physically zero-thickness of a gas-liquid interface is guaranteed. The governing equations for the time-dependent rising velocity and acceleration are derived.

**Keywords** Deformation, Heat, Fluid mechanics, Meshes, Numerical control, Simulation

**Paper type** Research paper



**Nomenclature**

$a$	= coefficient of discretisation equation	$\hat{\tau}$	= stress tensor
$J$	= Jacobian transformation number	$\alpha, \beta, \gamma$	= coordinate transformation parameters
$J_n, J_s, J_e, J_w$	= convection-diffusion fluxes at controlling cell face $n, s, e, w$	$\alpha_{uz}, \alpha_{pro}$	= relaxation factors
$n, s, e, w$	= cell faces of a control volume	$\Delta$	= finite difference operator
$N, S, E, W$	= neighbours of grid node $P$	$\xi, \eta$	= curvilinear coordinates
$Nu$	= Nusselt number	<i>Superscripts</i>	
$\bar{p}$	= pressure, Pa	(1)	= pertaining to block 1 (interior of gas-liquid interface)
$\vec{R}$	= position vector of $P$	(2)	= pertaining to block 2 (exterior of gas-liquid interface)
$r$	= axisymmetric radial coordinate	( $i$ )	= pertaining to block $i$ ( $i = 1, 2$ )
$R_{az}, R_m$	= curvature radii in the azimuthal and meridional surfaces, respectively	$K, K + 1$	= iteration steps
$Re$	= Reynolds number	'	= a correction
$S$	= source term	*	= an approximated value
$Sc$	= Schmidt number	<i>Subscripts</i>	
$Sh$	= Sherwood number	1, 2	= components in $\xi$ and $\eta$ directions, respectively
$t$	= time	a	= pertain to azimuthal surface
$u, v$	= velocity components along $x$ and $y$ , respectively, m/s	m	= pertain to meridional plane
$\bar{V}$	= volume of bubbles	$\vec{n}, \vec{t}$	= pertain to normal and tangential directions, respectively
$\vec{W}$	= vector of velocity	$N, S, E, W$	= pertaining to neighbours $N, S, E, W$
$We$	= Weber number	$n, s, e, w$	= pertaining cell faces $n, s, e, w$
$y$	= vertical coordinates	$Z - 1, Z$	= nodes on zonal boundary and on the first inner grid line, respectively
<i>Greek symbols</i>			
$\phi$	= general transport field variables	$\xi, \eta$	= partial derivative with respect to $\xi$ and $\eta$ , respectively
$\Phi_p, \Phi_\mu$	= ratios of fluid properties defined by equation (3)	$\phi$	= pertain to a general transport field variable $\phi$
$\Gamma$	= diffusion coefficient of $\phi$	$\infty$	= pertain to far field boundary
$\rho$	= density, kg/m <sup>3</sup>		
$\mu$	= dynamic viscosity of fluids, kg/m s		

**1. Introduction**

Momentum, heat and mass transfer between rising bubbles and the surrounding fluid are very popular and play important roles in engineering devices such as boilers and bubbly-flow-based chemical reactors. These transfer phenomena relevant to the gas-liquid interfaces are very complex but decisive to the productive capacity of the devices. The heat and fluid flows in both sides of the gas-liquid interface are conjugate, and the interface is deformable and of zero-thickness. A slight change of local mass, momentum and energy can cause great changes in the productive capacity of the devices. Because of the complexities, a single inert bubble is often employed to study the basic mechanism of the relevant transfer phenomena; and high fidelity for the flow

---

phenomena near the gas-liquid interface is the most important requirement for this kind of study.

For numerical analysis, because the properties of fluids usually exhibit step-changes at the interface, the predictions of heat and mass transfer and fluid flows must be performed simultaneously with the determination of the bubble shape. This problem is, therefore, very challenging for CFD researchers.

---

Mathematically, the simulation of a deformable single bubble is a moving boundary problem, which has a large body of successful strategies and numerical schemes. Most of these have been aimed at the difficulty of the tracking of time dependent moving boundaries. Reviews of these numerical strategies are presented by Shyy *et al.* (1996), Davidson and Rudman (2002) and Son (2005). Generally saying, the tracking of a moving boundary can use Lagrangian methods such as the arbitrary Lagrangian-Eulerian method (Hirt *et al.*, 1974), Eulerian methods such as volume of fluid (VOF) method (Hirt and Nichols, 1981; Davidson and Rudman, 2002), level set method (Osher and Sethian, 1988; Sussman *et al.*, 1994; Son *et al.*, 1999; Son, 2001, 2005) or Eulerian-Lagrangian methods (Univerdi and Tryggvason, 1992; Kan *et al.*, 1996; Bunner and Tryggvason, 1998; Tryggvason *et al.*, 2001). The front capturing methods such as VOF and level set, as reviewed by Shyy *et al.* (1996), use fixed Cartesian grids and can deal with strong deformation of bubbles. However, because the gas-liquid is captured, the numerical result has a non-physical thickness of more than a grid-space, the physical zero-thickness of a gas-liquid interface is not guaranteed by both the VOF and level set methods. This non-physical interface thickness combined with the rough treatments of interfacial forces, such as to change the tension force into a body force by the VOF method, can smear the fidelity of the flow details at the vicinity of the interface. These shortcomings of the VOF and level set methods are harmful for analysing the mechanism of heat and mass transfer at the interface. On the other hand, methods using a moving mesh are attractive because the moving boundary can be explicitly and accurately decided; and the physical zero-thickness of the interface is guaranteed by these methods. Ryskin and Leal (1984a, b) proposed to calculate the steady flow about single bubbles using a boundary-fitted mesh and Dandy and Leal (1989) later employed this strategy to study conjugate flows in liquid drops. These studies were restricted to the solving of steady Navier-Stokes equations in terms of vorticity and stream-function, and only orthogonal mesh systems can be used. Using orthogonal mesh is not a good option for calculating flows in complex geometries because of the mathematical difficulties in generating the strictly orthogonal mesh. In order to solve the problem, the present authors proposed to use a general non-orthogonal mesh method to calculate the steady heat and fluid flows in deformed bubbles (Lai *et al.*, 2003, 2004). In those calculations, we use a zoned body-fitted mesh to calculate the conjugate heat and flows in deformed bubbles. The zero-thickness of the gas-liquid interface is guaranteed and high fidelity of flow details near the interface is obtained.

This paper combines our non-orthogonal mesh method for steady conjugate flows in bubbles with a moving mesh algorithm, for flows in time-dependent geometries and also proposed by the authors Lai *et al.* (2002), to calculate the time-dependent conjugate heat and fluid flows inside and around a rising bubble. As a starting step, we will only present the method in an axisymmetric form and

calculate moderately deformable bubbles in this paper although the method has possibilities of expanding to be fully three-dimensional. This simplification is to highlight the advantage of obtaining high fidelity for the heat and fluid flows near the interface by the method.

The main contents of paper are organised in three sections. Section 2 presents the full algorithm. This starts in Section 2.1 from the governing equations. The discretisation of the basic equations using a non-staggered SIMPLE algorithm is presented in Section 2.2, where the Van Leer's (1979) total variation diminishing (TVD) scheme MUSCL is employed and the "space conservation law" (SCL) is invoked. Section 2.3 is the boundary conditions for the time-dependent conjugate flows relevant to the gas-liquid interface. The key step of using the interfacial boundary conditions to determine the interfacial velocity and the shape of the interface is presented in Section 2.4. Section 2.5 analyses the forces acting on the gas-liquid interface, and then presents the governing equations for the rising velocity and the acceleration. The solution algorithm for the whole problem is summarised in Section 2.6. Section 3 presents validation and application of the algorithm. This includes validating bubble shape at terminal state by available experimental data, and validating the calculated time-dependent rising velocity using results from an asymptotic model which is based on experiments, in Section 3.1. Based on this, Section 3.2 applies the algorithm to calculate the conjugate heat and fluid flows during time-dependent rising and deforming procedure of an inert bubble. Finally, the summary of the paper is given in Section 4.

## 2. Mathematical formulation

### 2.1 Governing equations

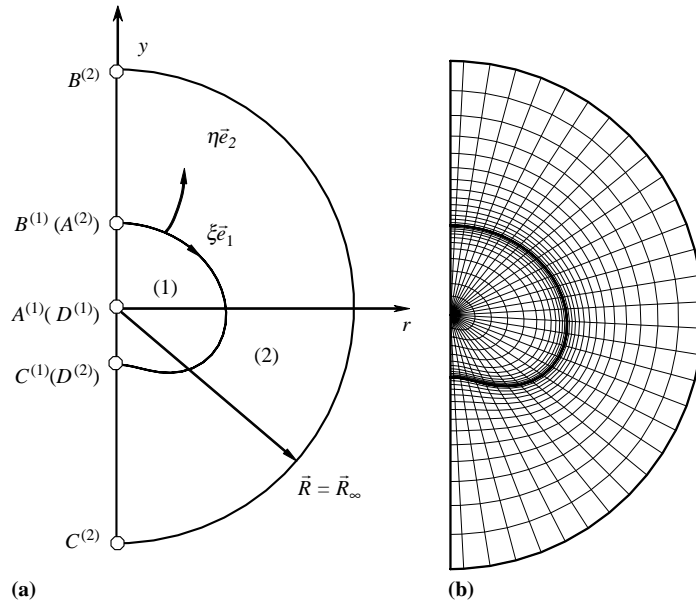
For simplicity, this paper studies the laminar and axisymmetric flows and assumes:

- Both the gas and the liquid are Newtonian fluids and the physical properties of the two fluids are constants; especially, the flows are incompressible.
- The dissolving of the bubble is sufficiently slow and the concentration of dissolved mass is dilute enough so that the Stefan flow can be ignored. In the meanwhile, the dissolution of the dispersed-phase is assumed to be a unidirectional procedure from the dispersed phase at the interface.
- There is no surface-active material.
- The flow inside the bubble is isothermal.

The non-inertial axisymmetric cylindrical coordinate system  $(r, y)$  is originated at the geometrical centre of the bubble,  $O$ ;  $r$  and  $y$  are the radial and vertical coordinates, respectively, (shown in Figure 1(a)). A two-block computational domain is separated by a zonal boundary fitting the bubble surface profile. Denote the interior and exterior blocks and all parameters pertaining to them with superscripts (1) and (2), respectively, the normalised governing equations for the heat and fluid flows are as following:

$$\frac{\partial(r\phi)}{\partial t} + \frac{\partial}{\partial r}(ru\phi) + \frac{\partial}{\partial y}(rv\phi) = \frac{\partial}{\partial r} \left( r\Gamma \frac{\partial \phi}{\partial r} \right) + \frac{\partial}{\partial y} \left( r\Gamma \frac{\partial \phi}{\partial y} \right) + rS, \quad (1)$$

where:



**Figure 1.**  
Zoned computational domain and grids:  
(a) computational domain;  
and (b) grids distribution

$$\phi = \begin{bmatrix} 1 \\ u \\ v \\ T \\ c \end{bmatrix}, \quad \Gamma = \begin{bmatrix} 0 \\ \frac{1}{Re^{(i)}} \\ \frac{1}{Re^{(i)}} \\ \frac{1}{Re^{(i)}Pr} \\ \frac{1}{Re^{(i)}Sc} \end{bmatrix}, \quad S = \begin{bmatrix} 0 \\ -\frac{\partial b^{(i)}}{\partial r} + \frac{1}{Re^{(i)}} \left(-\frac{u}{r^2}\right) \\ -\frac{\partial b^{(i)}}{\partial y} - \frac{d_{ref}}{V_{ref}^2} a_O(t) \\ 0 \\ 0 \end{bmatrix} \quad (i = 1 \text{ and } 2),$$

$u$  and  $v$  are Cartesian components of  $\vec{W}$ , the velocity of flow in the non-inertial coordinates system;  $T$  is temperature;  $c$  is the concentration of species. The Reynolds number  $Re^{(i)}$  is based on the referential velocity  $V_{ref}$ , diameter  $d_{ref}$ ,  $\rho^{(i)}$  and  $\mu^{(i)}$ ;  $Pr$  and  $Sc$  are Prandtl and Schmidt numbers;  $\alpha_o(t)$  is the acceleration of the rising bubble and will be discussed later. For density  $\rho$  and viscosity  $\mu$ , we have:

$$\Phi_\rho = \frac{\rho^{(1)}}{\rho^{(2)}}, \quad \Phi_\mu = \frac{\mu^{(1)}}{\mu^{(2)}}, \quad Re^{(1)} = Re^{(2)} \frac{\Phi_\rho}{\Phi_\mu}, \quad (2)$$

where  $\Phi_\rho$  and  $\Phi_\mu$  are the ratio of density and viscosity between the fluids in both sides of the gas-liquid interface.

From the point of view of a chemical reaction in bubbly flows, it is a procedure of changing electrons between ions; this procedure always occurs in the liquid side where

the dissolved gas can freely ionise, and the procedure may accompanied by heat transfer. Because of these, the heat and mass transfer could be regarded as procedures between bubble surface and the liquid and, therefore, for the temperature field  $T$  and concentration field  $c$ , we only consider them outside of the bubble surface (i.e. the liquid side) in this paper.

### 2.2 Discretisation of equations

In a Lagrangian (time-dependent) non-orthogonal boundary-fitted coordinates system ( $t, \xi, \eta$ ), equation (1) changes into:

$$\begin{aligned} \frac{\partial(rJ\phi)}{\partial t} + \frac{\partial}{\partial \xi} \left\{ r \left[ G_r^1 \phi - \frac{\Gamma}{J} \left( \alpha \frac{\partial \phi}{\partial \xi} - \beta \frac{\partial \phi}{\partial \eta} \right) \right] \right\} \\ + \frac{\partial}{\partial \eta} \left\{ r \left[ G_r^2 \phi - \frac{\Gamma}{J} \left( -\beta \frac{\partial \phi}{\partial \xi} + \gamma \frac{\partial \phi}{\partial \eta} \right) \right] \right\} = rJS, \end{aligned} \quad (3)$$

where  $\alpha, \beta, \gamma$  are metrics of the curvilinear coordinates while  $J$  is the Jacobian determinant:

$$\alpha = r_\eta^2 + y_\eta^2, \quad \beta = r_\xi r_\eta - y_\xi y_\eta, \quad \gamma = r_\xi^2 + y_\xi^2, \quad J = r_\xi y_\eta - y_\xi r_\eta; \quad (4)$$

$G_r^1$  and  $G_r^2$  are the contravariant components of the relative velocity  $\vec{W}_r$ :

$$\begin{aligned} \vec{W}_r = \vec{W} - \vec{W}_g, \quad G_r^1 = (u - u_g)y_\eta - (v - v_g)r_\eta, \\ G_r^2 = (v - v_g)r_\xi - (u - u_g)y_\xi; \end{aligned} \quad (5)$$

$u_g$  and  $v_g$  are Cartesian components of grid velocity  $\vec{W}_g$ :

$$u_g = \frac{dx}{dt}, \quad v_g = \frac{dy}{dt}. \quad (6)$$

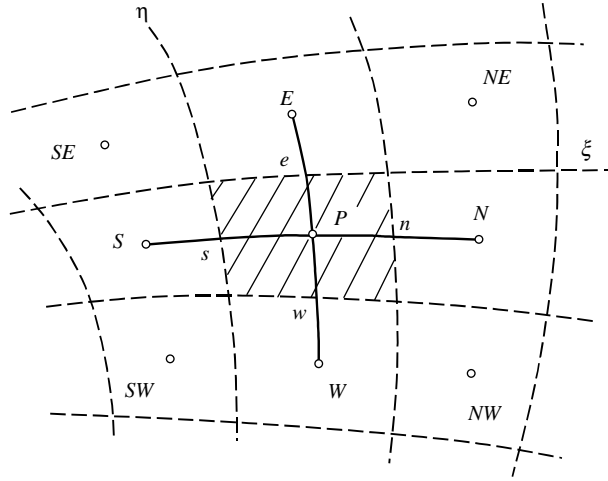
Integrating equation (1) over the shaded control volume shown in Figure 2, we have:

$$\frac{(Jr\phi)_P - (Jr\phi)_P^o}{\Delta t} \Delta \xi \Delta \eta + J_n - J_s + J_e - J_w = (JrS)_P \Delta \xi \Delta \eta. \quad (7)$$

To calculate the cell face fluxes  $J_n, J_s, J_e$  and  $J_w$ , Van Leer's (1979) TVD scheme MUSCL is employed and implemented in a form of "deferred correction" (1974) to the upwind approximation by introducing an additional source term  $S_{DC}$ . The final form of discretisation is:

$$a_P \phi_P = a_N \phi_N + a_S \phi_S + a_E \phi_E + a_W \phi_W + b + S_{DC}, \quad (8)$$

where:



**Figure 2.**  
Control volume for  
discretisation

$$\left\{ \begin{array}{l}
 a_p = a_N + a_S + a_E + a_W + (Jr\Delta\xi\Delta\eta)/\Delta t \\
 b = (JrS)_P\Delta\xi\Delta\eta + (Jr\phi)^o\Delta\xi\Delta\eta/\Delta t \\
 S_{DC} = \frac{1}{2} \left\{ G_{r,n}^1 G_{r,n}^{1+} \min \text{mod} (\Delta_n, \Delta_n^-) - G_{r,n}^1 G_{r,n}^{1-} \min \text{mod} (\Delta_n, \Delta_n^+) \right. \\
 \quad - G_{r,s}^1 G_{r,s}^{1+} \min \text{mod} (\Delta_s, \Delta_s^-) + G_{r,s}^1 G_{r,s}^{1-} \min \text{mod} (\Delta_s, \Delta_s^+) \\
 \quad + G_{r,e}^2 G_{r,e}^{2+} \min \text{mod} (\Delta_e, \Delta_e^-) - G_{r,e}^2 G_{r,e}^{2-} \min \text{mod} (\Delta_e, \Delta_e^+) \\
 \quad \left. - G_{r,w}^2 G_{r,w}^{2+} \min \text{mod} (\Delta_w, \Delta_w^-) + G_{r,w}^2 G_{r,w}^{2-} \min \text{mod} (\Delta_w, \Delta_w^+) \right\} \\
 \Delta_f^- = \phi_P - \phi_{P-1}, \quad \Delta_f = \phi_{P+1} - \phi, \quad \Delta_f^+ = \phi_{P+2} - \phi_{P+1}, \quad G^\pm = \frac{1 \pm \text{sgn}(G)}{2} \\
 \min \text{mod}(a, b) = \text{sgn}(a) \max\{0, \min[|a|, y \text{sgn}(a)]\}
 \end{array} \right.$$

$a_p, a_N, a_S, a_E$  and  $a_W$  are calculated by the first-order upwind scheme (Patankar, 1980),  $S_{DC}$  is the additional source term introduced by the using of the deferred correction.

It should be specially mentioned that the determinant of Jacobian transform  $J$  in equations (7) and (8) cannot be simply calculated according to equation (4) because the so-called SCL (Trulio and Trigger, 1961; Thomas and Lombard, 1979) must be satisfied. The mathematical description of the SCL can be obtained from equation (3) by setting  $\phi = 1, \Gamma = 0, S = 0, r = 1$ , and  $\bar{W}_r = -\bar{W}_g (\bar{W} = 0)$ , which results in:

$$\frac{\partial J}{\partial t} = \frac{\partial G_g^1}{\partial \xi} + \frac{\partial G_g^2}{\partial \eta}. \tag{9}$$

Equation (9) implies that the time derivative of the computational cell volume is related to the grid velocity. To satisfy the SCL, Lai *et al.* (2002) proposed to calculate the grid velocity using equation (6) and then update  $J$  through equation (9); an explanation

for the SCL has also been given by the present authors in that study but omitted here to avoid duplication.

The basic equations of heat and fluid flows will be solved by using the SIMPLE method with a non-staggered grid arrangement (Lai and Yan, 2001).

### 2.3 Boundary conditions

The boundary conditions are imposed as following:

At the axis of symmetry ( $x = 0$ ):

$$u = 0, \quad \frac{\partial v}{\partial r} = 0, \quad \frac{\partial p^{(i)}}{\partial r} = 0, \quad \frac{\partial T}{\partial r} = 0, \quad \frac{\partial c}{\partial r} = 0; \quad (10)$$

at the free stream (far field, i.e. at  $\vec{R} = \vec{R}_\infty$  in Figure 1(a)):

$$u = 0, \quad v = -V_O(t), \quad p^{(2)} = p_\infty, \quad T^{(2)} = T_\infty, \quad c^{(2)} = c_\infty; \quad (11)$$

at the interface:

$$W_{\vec{n}}^{(1)} = W_{\vec{n}}^{(2)} = 0; \quad (12)$$

$$W_{\vec{t}}^{(1)} = W_{\vec{t}}^{(2)}, \quad (13)$$

$$\hat{\tau}_{\vec{t}}^{(1)} \Phi_\rho = \hat{\tau}_{\vec{t}}^{(2)}, \quad (14)$$

$$\hat{\tau}_{\vec{n}}^{(1)} \Phi_\rho + \frac{1}{We} \left( \frac{1}{R_m} + \frac{1}{R_a} \right) = \hat{\tau}_{\vec{n}}^{(2)}, \quad (15)$$

$$T^{(1)} = T^{(2)} = T_{\text{Sat}}, \quad c^{(1)} = c^{(2)} = c_{\text{Sat}}, \quad (16)$$

where the subscripts “ $\vec{n}$ ” and “ $\vec{t}$ ” denote the unit normal and tangential vectors of the interface, respectively; “sat” denotes variables at status of saturation;  $W_{\vec{n}}$  and  $W_{\vec{t}}$  are normal and tangential components of interfacial velocity;  $\hat{\tau}$  is the fluid internal stress tensor whose components are  $\tau_{\vec{n}}$  and  $\tau_{\vec{t}}$ ;  $We$  is Weber number. The balance of normal forces acting at the bubble surface is shown in Figure 3(a), where  $R_m$  and  $R_a$  are curvature radii in the meridional plane and the azimuthal surface, respectively, and calculated as follows:

$$\frac{1}{R_m} = \frac{y_\xi r_{\xi\xi} - r_\xi y_{\xi\xi}}{(r_\xi^2 + y_\xi^2)^{3/2}}, \quad \frac{1}{R_a} = -\frac{y_\xi}{r(r_\xi^2 + y_\xi^2)^{3/2}}. \quad (17)$$

In the boundary conditions at the interface, equations (12) and (13) are the kinematic conditions, describing no penetration across the interface and the continuity of tangential velocity, respectively; equations (14) and (15) are the dynamic conditions, the continuity of tangential stress and the balance of normal stress (notice different referential density has been used in the two sides of the interface); conditions in equation (16) are the first kind boundary conditions for temperature and concentration.



2.4 Interfacial treatments and a modified “Ryskin-Leal” method

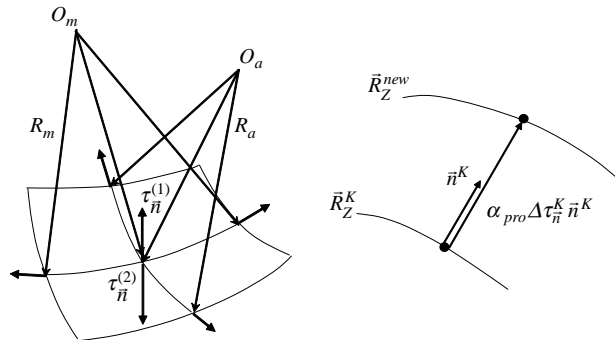
Except the unknown value  $V_o(t)$ , which will be discussed in the next section, boundary conditions (10), (11) and (16) are straightforward to be posed because these equations are very simple and can be used to impose the explicit boundary values of primitive variables. The treatments of conditions (12)-(15) are the major difficulties because they are genuinely transient conditions for determining bubble shape and interfacial velocities. The stresses in equations (14) and (15) are calculated as following:

$$\tau_t^{(i)} = \frac{1}{Re^{(i)}\gamma J} \left[ r_\xi \gamma \frac{\partial u}{\partial \eta} + y_\xi \gamma \frac{\partial v}{\partial \eta} - (r_\xi \beta + y_\xi J) \frac{\partial u}{\partial \xi} + (r_\xi J - y_\xi \beta) \frac{\partial v}{\partial \xi} \right], \quad (18)$$

$$\tau_n^{(i)} = -p^{(i)} + \frac{2}{Re^{(i)}\gamma J} \left[ \beta \left( y_\xi \frac{\partial u}{\partial \xi} - r_\xi \frac{\partial v}{\partial \xi} \right) + \gamma \left( r_\xi \frac{\partial v}{\partial \eta} - y_\xi \frac{\partial u}{\partial \eta} \right) \right]. \quad (19)$$

It is obvious that equations (18) and (19) are neither explicit functions of time nor first kind Dirichlet conditions of interfacial velocity. Special treatments must be proposed so as to decide the bubble shape and interfacial velocity. In the current study, the “continuous stress method” for steady flows in bubbles, proposed by the authors Lai *et al.* (2003), is further employed to obtain interfacial velocity from equations (12) to (14), making use of the implicit characteristics of these equations. In other words, as no explicit time appears in equations (12)-(14), the determination of interfacial velocity at every instant can be carried out according to the “continuous stress method” for steady problems; the details of the method are described by Lai *et al.* (2003).

In the meanwhile, the bubble shape at each instant must be determined. Ryskin and Leal (1984a, b) reviewed some possible routes and proposed a simple and indirect method of determining the interface shape by using equation (15). In their method, the shape of an interface is modified at each iteration step by moving the points of the surface in local normal direction by an amount proportional to the pressure difference. Owing to the restraint of using orthogonal meshes, the interface updating had to be done indirectly by changing the Lamé metric coefficients of the coordinates system; possible instability of numerical calculation is inevitably introduced. In order to sort out the problem, Salvador (1994) proposed to decide the interface shape by directly modifying the coordinates of the points. Salvador (1994) and Raymond and Rossant (2000) studied the slightly deformed bubbles using this method. Although these



**Figure 3.** Determination of the new interface position: (a) balance of normal stress; and (b) update of interfacial profile

applications are for studying steady bubbles using “external flow” models, their methods to determine the interface shape can be modified to our current study.

Figure 3(b) shows an initial shape,  $\vec{R}_Z^K$ , of bubble profile at a certain physical instant. It could be an intermediate result and, therefore, further iterations must be carried out. The imbalance of normal forces on the current iteration (denoted by script  $K$ ):

$$\Delta\tau_{\vec{n}}^K = \tau_{\vec{n}}^{(2)K} - \left[ \tau_{\vec{n}}^{(1)K} \Phi_\rho + \frac{1}{We} \left( \frac{1}{R_m} + \frac{1}{R_a} \right) \right]^K, \quad (20)$$

is used to predict the interface shape. That is:

$$\vec{R}_Z^{\text{new}} = \vec{R}_Z^K + \alpha_{\text{pro}} \Delta\tau_{\vec{n}}^K \vec{n}^K, \quad (21)$$

where  $\vec{n}^K$  is the unit normal vector of the interface. Because the bubble profile is explicitly updated in equation (21), and the curvature radii  $R_m$  and  $R_a$  generally contains second derivatives of the coordinates, the calculation will be unstable and an under-relaxation factor  $\alpha_{\text{pro}}$  is introduced. The value of  $\alpha_{\text{pro}}$  is determined by numerical experiment, its typical value is of the magnitude of  $10^{-3}$ - $10^{-2}$ .

Except using the low valued under-relaxation factor  $\alpha_{\text{pro}}$ , a smoothing method has to be applied occasionally to filter the high frequency waves generated during updating the bubble profile. Discrete filters (Sagaut and Grohens, 1999) maybe applicable but the harmonious decomposition to the imbalance of normal stress, suggested by Salvador (1994), is more attractive for the current study because of its easy controlling of cut-off wave. This harmonious decomposition is adopted in our study and briefly introduced in the following.

Considering the imbalance of normal forces,  $\Delta\tau_{\vec{n}}$ . It is a function of  $\xi$ . Because of the axisymmetry assumption,  $\Delta\tau_{\vec{n}}$  can be further treated as a periodical function in the zone of  $[-\xi_{\text{max}}, \xi_{\text{max}}]$ . A harmonious decomposition can be carried out by expanding  $\Delta\tau_{\vec{n}}$  using the Fourier series as following:

$$\Delta\tau_{\vec{n}}(\xi) = \frac{a_0}{2} + \sum_{k=1}^{\infty} [a_k \cos(k\omega\xi) + b_k \sin(k\omega\xi)], \quad (22)$$

where  $\omega = \pi/\xi_{\text{max}}$ :

$$\begin{cases} a_k = \frac{1}{\xi_{\text{max}}} \int_{-\xi_{\text{max}}}^{\xi_{\text{max}}} \Delta\tau_{\vec{n}}(\xi) \cos(k\omega\xi) d\xi, & k = 0, 1, 2, 3, \dots \\ b_k = \frac{1}{\xi_{\text{max}}} \int_{-\xi_{\text{max}}}^{\xi_{\text{max}}} \Delta\tau_{\vec{n}}(\xi) \sin(k\omega\xi) d\xi, & k = 1, 2, 3, \dots \end{cases}$$

For calculations based on discretisation:

$$\begin{cases} a_k = \frac{1}{\xi_{\text{max}}} \sum_{\xi=-\xi_{\text{max}}}^{\xi_{\text{max}}} \Delta\tau_{\vec{n}}(\xi_i) \cos(k\omega\xi_i) \Delta\xi_i, & k = 0, 1, 2, 3, \dots \\ b_k = \frac{1}{\xi_{\text{max}}} \sum_{\xi=-\xi_{\text{max}}}^{\xi_{\text{max}}} \Delta\tau_{\vec{n}}(\xi_i) \sin(k\omega\xi_i) \Delta\xi_i, & k = 1, 2, 3, \dots \end{cases}$$

According to Salvador's (1994) suggestion, the maximum order of the Fourier series can be set as  $k_{\max} = 5 \sim 6$ .

The new position of the interface,  $\vec{R}_Z^{\text{new}}$  determined by equation (21) is not an exact value; the conservation of the bubble volume is employed here to determine exact position at the  $K + 1$ th iteration. Define a volume-scaling factor  $\mathfrak{R}$  as following:

$$\mathfrak{R} = \left( \frac{V^K}{V^{\text{new}}} \right)^{1/3}, \quad (23)$$

where  $V^K$  and  $V^{\text{new}}$  are the volumes enclosed by the profiles  $\vec{R}^K$  and  $\vec{R}^{\text{new}}$ , respectively. The updated position of the interface is, therefore, decided as:

$$\vec{R}_Z^{K+1} = \mathfrak{R} \vec{R}_Z^{\text{new}}. \quad (24)$$

The two-step method in equations (21) and (24) of determining interface shape differs from Ryskin and Leal's (1984a, b) method by updating the bubble profile directly and is called as a "modified Ryskin-Leal method".

Every time after the bubble profile is updated, the grids for calculation must be adjusted so as to map the deformed bubble profile. Because the origin of the non-inertial coordinates system has been fixed at the bubble's geometrical centre, the outer boundary of the computational domain ( $\vec{R} = \vec{R}_\infty$  in Figure 1(a)) can be retained during the grid adjustment. Therefore, the procedure for adjusting the grids is actually re-generating the grids in the two single-connected domains  $A^{(1)}B^{(1)}C^{(1)}D^{(1)}$  and  $A^{(2)}B^{(2)}C^{(2)}D^{(2)}$ , respectively; the single-connected domain grid-generation is carried out by using the well-known TTM method proposed by Thompson *et al.* (1974), where TTM is the abbreviation of these researchers' surnames. Figure 1(b) shows an illustration of the grid distribution, which are stretched close to the bubble profile so as to highlight the flow details there.

### 2.5 Rising velocity

In order to calculate the time-dependent bubble rising described by the governing equations and boundary conditions, the unknown time-dependent velocity and acceleration of bubble geometrical centre,  $V_o(t)$  and  $a_o(t)$  appeared in equations (11) and (1) and with respected to the earth, must be decided; and additional independent equations must be derived and coupled with the Navier-Stokes equations. This paper decides the rising velocity and acceleration according to the forces acting on the bubble.

Consider a single bubble rising in an unbounded liquid. The integration of the normal and tangential forces over the bubble results in the vectorial summation of the buoyancy and drag forces:

$$F_y = F_B - F_D = \int_0^{\xi_{\max}} 2\pi r \left( r_\xi \tau_{\bar{n}}^{(2)} + y_\xi \tau_{\bar{t}}^{(2)} \right) d\xi, \quad (25)$$

where  $F_B$  and  $F_D$  are the buoyancy and drag forces, respectively.

Except the surface forces, the gravity acts on the bubble in the form of a body force:

$$F_g = \rho^{(1)} V g. \quad (26)$$

Therefore, the acceleration of the bubble satisfies the following equation:

$$\rho^{(1)} \nabla \cdot a_O(t) = F_y - F_g = F_B - (F_D + F_g). \quad (27)$$

Time-dependent  
heat and fluid  
flows

The rising velocity of the bubble can be given by the integration of  $a_O(t)$ :

$$V_O(t) = V_O(t_0) + \int_{t_0}^t a_O(t) dt. \quad (28)$$

429

Give the initial value of  $V_O(t_0)$  and proper initial fields, the mathematical model of the current problem becomes well posed and can be solved.

### 2.6 Solution algorithm

A full numerical procedure to calculate the time-dependent rising of a single bubble introduced into an unbounded liquid is summarised as follows:

- (1) define a far field boundary  $\vec{R} = \vec{R}_\infty$  where the flow blockage effects due to the bubble can be neglected;
- (2) give an initial field and a time step  $\Delta t$ ;
- (3) in time level  $t^{n+1} = t^n + \Delta t$ , determine  $a_O(t^{n+1})$  and  $V_O(t^{n+1})$  according to equations (26) and (27), respectively;
- (4) solve fluid flows inside and around a given shape of bubble, subject to the boundary conditions (12)-(14), by using the “continuous stress method”;
- (5) update the bubble profile according to the “modified Ryskin-Leal method”;
- (6) regenerate body-fitted mesh to map the new bubble-profile, calculate the grid velocity  $u_g$  and  $v_g$  according to equation (6) using implicit difference with respect to time, updating the Jacobian  $J$  using equation (9) and recalculate the coefficients of discretised equation (8);
- (7) return to step (4) and carrying out iterations until equation (15) is satisfied;
- (8) return to step (3) to update  $a_O(t^{n+1})$  and  $V_O(t^{n+1})$  if they are still changing with the updating of bubble profile for  $t^{n+1}$ ; otherwise, convergence of fluid flow can be declared for time-level  $t = t^{n+1}$ ;
- (9) solve the heat and mass transfer problem for time-level  $t = t^{n+1}$ , subjects to boundary conditions in equation (16); and
- (10) check the variation:

$$|V_O(t^{n+1}) - V_O(t^n)| \leq \varepsilon_{\text{ref}}, \quad (29)$$

if inequality (29) is satisfied, the rising bubble has arrived at its terminal state and the calculation can be stopped; otherwise, return to step (2) to calculate the next time-level.


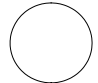

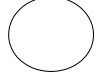

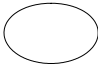

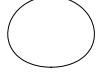

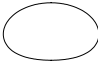
The criterion  $\varepsilon_{\text{ref}}$  defined by inequality (29) is an important parameter for calculation of time-dependent rising and must be valued on the magnitude of  $O(10^{-3})$  or even higher.

### 3. Numerical results

#### 3.1 Validation

The bubbles measured by Raymond and Rossant (2000) are employed to validate the current numerical procedure. Corresponding to the experimental conditions (at room temperature, 20°C, and in atmosphere), the ratios of fluid properties are set as  $\Phi_\rho = 1 : 800$  and  $\Phi_\mu = 1 : 100$ . The outer boundary is assigned at 50 times of the equivalent bubble radius where the blockage effects of the bubble can be neglected (Lai *et al.*, 2003). In order to eliminate the grid-dependency of the numerical results, three meshes are tested with mesh 1, block 1 =  $52 \times 32$ , block 2 =  $62 \times 62$ ; mesh 2, block 1 =  $82 \times 42$ , block 2 =  $90 \times 82$ ; and mesh 3, block 1 =  $162 \times 62$ , block 2 =  $182 \times 162$ . Five cases are calculated and the results are shown in Figure 4 and Table I.

Table I compares the bubble aspect ratios,  $h/w$ , where  $h$  and  $w$  are the height and width of the bubble, respectively. The results obtained by mesh 1 have maximum relative errors in all the five cases while the difference in the results of mesh 2 and mesh 3 are negligible. For the case of  $(Re^{(2)}, We) = (28, 3.7)$ , the error between the

$(Re^{(2)}, We)$	Experiments (Raymond and Rossant, 2000)	Present Result
(0.5, 0.15)		
(3.7, 1.0)		
(28, 3.7)		
(1.9, 1.3)		
(9.3, 4.0)		

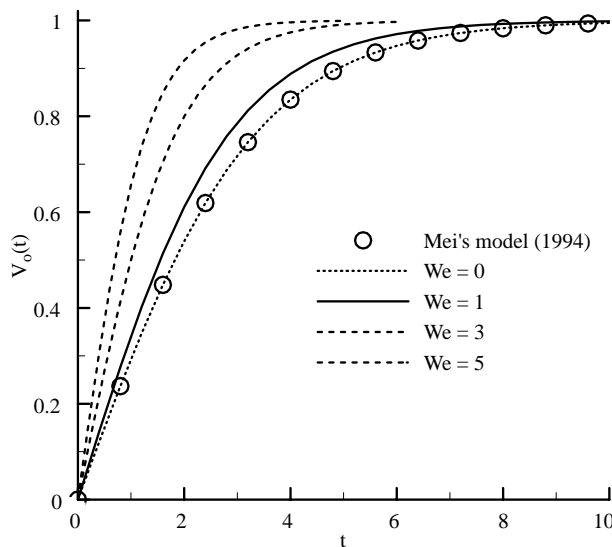
**Figure 4.**  
Comparison of bubble shapes

$(Re^{(2)}, We)$	$h/w$ experiments (Raymond and Rossant, 2000)	$h/w$ mesh 1	$h/w$ mesh 2	$h/w$ mesh 3
(0.5, 0.15)	0.98	0.951	0.975	0.977
(3.7, 1.00)	0.87	0.848	0.877	0.875
(28, 3.70)	0.64	0.623	0.640	0.638
(1.9, 1.30)	0.84	0.862	0.836	0.835
(9.3, 4.00)	0.57	0.613	0.601	0.599

**Table I.**  
Comparison between  
computed and measured  
aspect ratios

experiment and calculation with mesh 1 is about 2.66 per cent, which means mesh 1 is not fine enough to produce grid-independent results; on the other hand, the discrepancies between numerical and experimental  $h/w$  values for meshes 2 and 3 are less than  $5 \times 10^{-3}$  for this case. Except the final case shown in Table I, both meshes 2 and 3 have obtained excellent agreement with experiment and difference of the results obtained by the two meshes in all cases are of the magnitude of  $10^{-3}$ , therefore, mesh 2 can be regarded as fine enough to provide a grid independent solution and it will be employed in the left calculations in this paper. The final case in Table I has a discrepancy of 5 per cent for both mesh 2 and mesh 3; this deviation between experiment and calculation is possibly not a result of numerical error, but is more likely to be a result of the asymmetry of the bubble profile for this case, as pointed out by Raymond and Rossant (2000). Despite this deviation, the agreements between calculation and experiments are good in general; these agreements are also confirmed by the comparison of the calculated bubble shapes with their photographs given by Raymond and Rossant (2000), as shown in Figure 4.

More validations of the algorithm by steady conjugate flow at terminal state of rising bubbles have been presented in our previous papers (Lai *et al.*, 2003, 2004). For the simulation of a bubble at the acceleration stage, we validate the prediction of time-dependent rising velocity against the results from the asymptotic model for spherical bubbles (Mei *et al.*, 1994), which is based on the summary and analyse of a large variety of experimental data. Figure 5 shows the time history of dimensionless rising velocity for the air bubbles rising in hot water (100°C and 1 atm) at  $Re^{(2)} = 200$ ,  $\Phi_\rho = 1 : 800$ ,  $\Phi_\mu = 1 : 100$ ,  $Pr^{(2)} = 2$  and  $Sc^{(2)} = 500$ . It can be seen that the present result for spherical bubble ( $We = 0$ ) has a perfect agreement with the asymptotic model. In addition, Figure 5 also shows the lower Weber number, the closer to the asymptotic model data. This is because the bubbles at lower Weber number have



**Figure 5.**  
Time history of rising  
velocity of bubbles at  
 $Re^{(2)} = 200$

stronger gas-liquid interface tension and, therefore, weaker deformation, their shapes are closer to be spherical.

In the meanwhile, the results show that at a given exterior Reynolds number, a bubble at the bigger Weber number needs the shorter dimensionless time to arrive at its terminal state. Krishna and Baten (1999) and Sato *et al.* (2000) observed that bubbles at large Weber number values had oscillatory rising velocity and zig-zag trajectories. These phenomena are not found in our calculation because our Weber number is small and the flow around the bubble is laminar.

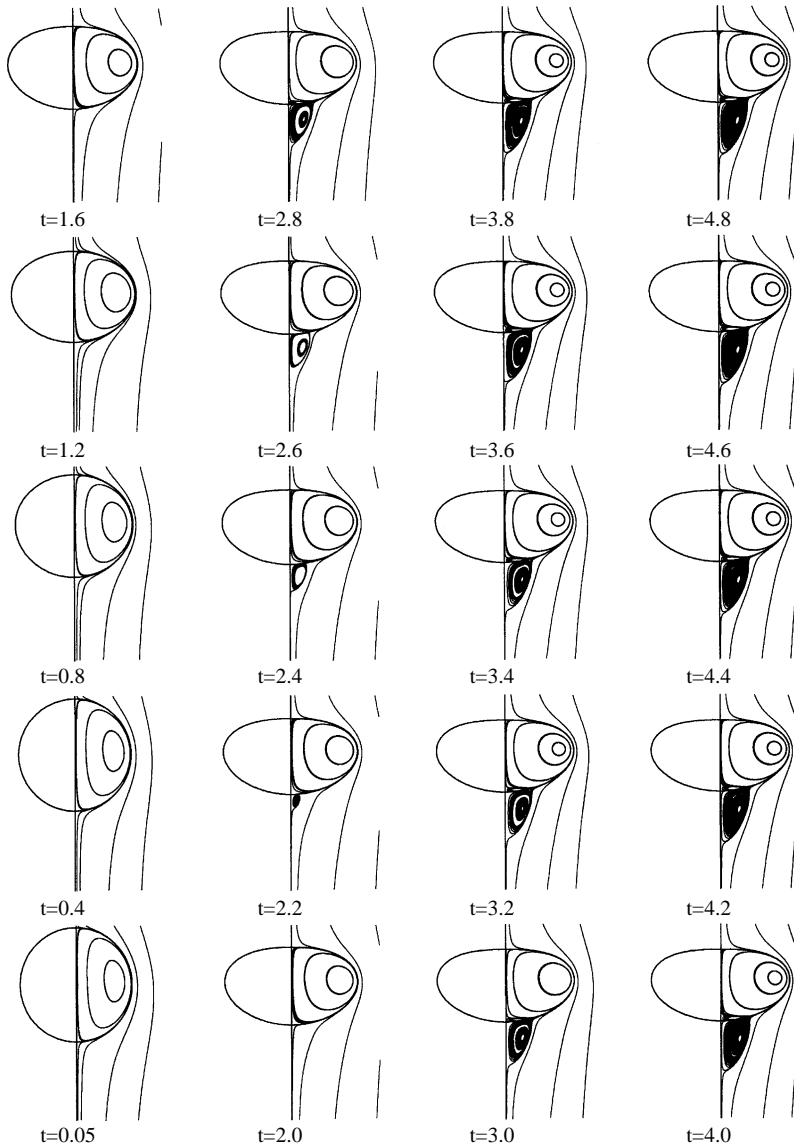
### 3.2 Bubble dynamics during acceleration

Nine cases, whose terminal Reynolds and Weber numbers are  $(Re^{(2)}, We) = [10, 50, 200] \times [1, 3, 5]$ , are calculated in this study. The computational domain and mesh are the same with previous calculations. Again, the fluid properties are set to those of air bubble rising in hot water (100°C and 1 atm).

Figure 6 shows the evolution of bubble shape and flow structure for  $(Re^{(2)}, We) = (200, 5)$ , where the streamlines are expressed in term of the relative velocity  $\bar{W}_r$ . Outside the bubble, flow separation from the bubble surface is observed during the bubble rising, at non-dimensional time  $t = 2.1$ . The ring vortex grows with time but attached to the bottom of the bubble all the time; so vortex shedding does not occur and the rising path remains smooth. For our simulated cases, very weak flow separation at the rear of the bubble is also observed at  $(Re^{(2)}, We) = (50, 5)$ . These two cases are not in the range of Reynolds and Weber numbers studied by Krishna and Baten (1999) and Sato *et al.* (2000). So it is not a surprise for the smooth rising velocity shown in Figure 5. Inside the bubble, when flow separation occurs, the circulation changes from a single ring vortex to a structure with a pair of counter rotating ring vortices. Figure 6 also shows that the deformation of bubbles occurs mainly at the early stage of the acceleration, namely, before  $V_o(t)$  arrives at about 80 per cent of its value at terminal state; later than this, the deformation is very slow. Relative to this early-stage bubble deformation, the onset of separation is later.  $V_o(t)$  at the onset of separation ( $t = 2.1$ ) is already nearly 95 per cent of its terminal value, as shown in Figure 5. This phenomenon may prove that separation is the accumulation of vortices, which is indicated by Ryskin and Leal (1984a, b). Because of the curvature and no-slip boundary at the gas-liquid interface, vorticity can be generated and be advected to the rear of the bubble and results in flow separation. This procedure takes time so the wake vortex can only be observed at the late stage of acceleration.

In the meanwhile, the late onset of separation raises a requirement for the convergent criterion  $\varepsilon_{\text{ref}}$  defined by inequality (29). In our calculation, this criterion is set at  $\varepsilon_{\text{ref}} = 1 \times 10^{-4}$  so as to expose all details of flow phenomena.

Figures 7 and 8 show the time-dependent development of dimensionless temperature and concentration fields. In these figures, the propagations of the temperature and concentration are seen to happen at the early stage of bubble rising when deformation quickly occurs. The temperature field has stronger diffusion while the concentration is more dominantly controlled by convection. This can be clearly observed at the very beginning of bubble-rise, where the contours of temperature are almost fore-aft symmetric while the concentration fields are obviously asymmetric.



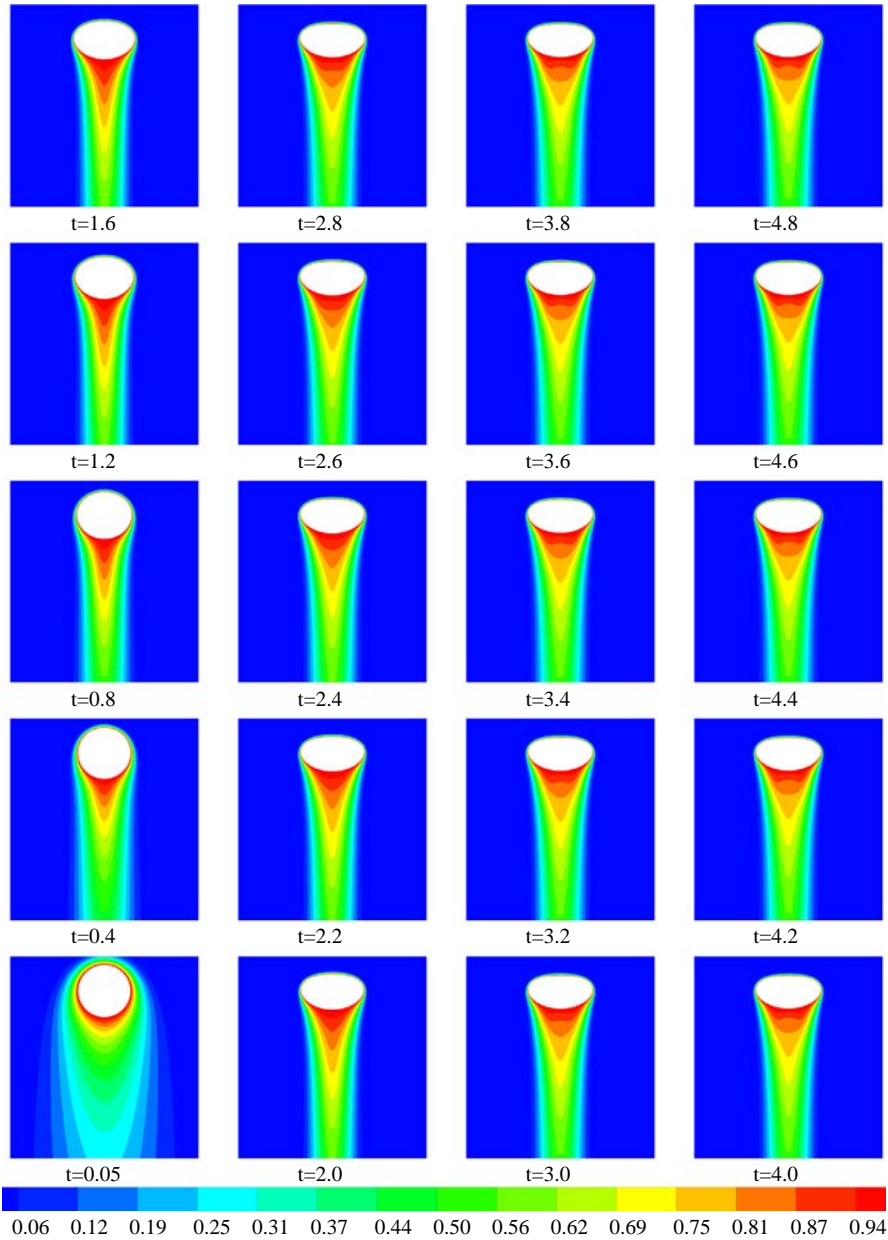
**Figure 6.**  
Evolution of bubble shape  
and flow structure at  
 $Re^{(2)} = 200$ ,  $We = 5$

In the meanwhile, the concentration wake zone behind the bubble is narrow and long while that of temperature is wide and short.

Define the local Nusselt and Sherwood numbers as following:

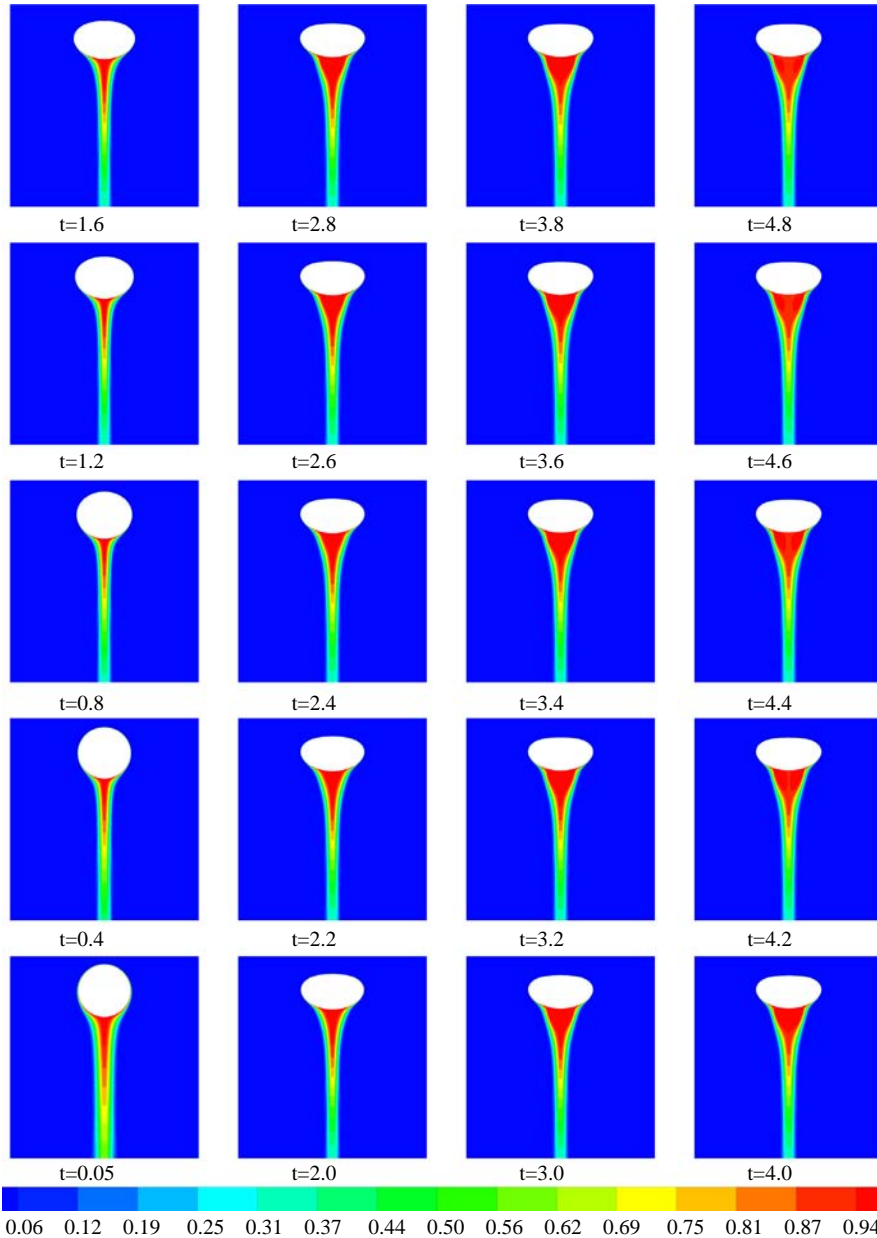
$$Nu = -\frac{\partial T}{\partial n}, \quad Sh = -\frac{\partial c}{\partial n}, \quad (30)$$





**Figure 7.**  
Development of  
temperature field for a  
rising bubble at  
 $Re^{(2)} = 200$ ,  $We = 5$

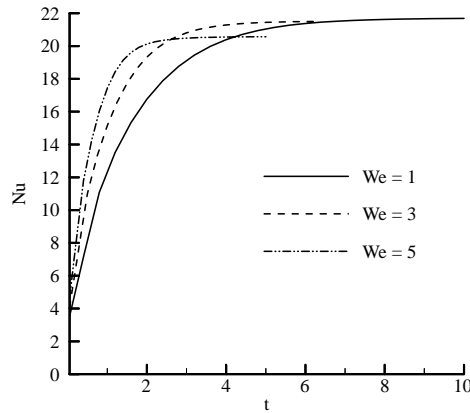
where  $\vec{n}$  is the unit local normal vector of the bubble surface and pointing into the liquid side. The time-dependent changes of  $Nu$  and  $Sh$ , averaged along the bubble surface, are shown in Figures 9 and 10. These parameters have a same story with the time-dependent rising velocity, that is, the parameters increase quickly at the



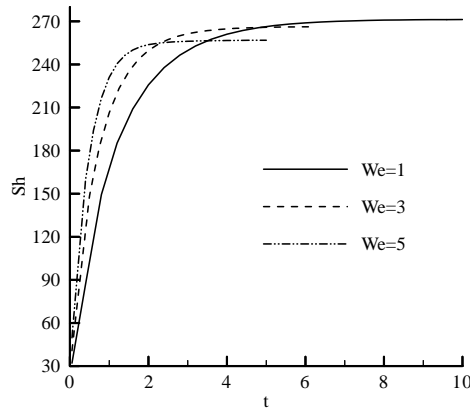
**Figure 8.**  
Development of  
concentration field for a  
rising bubble at  
 $Re^{(2)} = 200$ ,  $We = 5$

early stage of bubble acceleration while the increase for late stage is very slow. It should be noticed that even at the instant when the bubble enters the hot liquid, the averaged Nusselt and Sherwood numbers are not zero because of the diffusion effects.

**Figure 9.**  
Time history of averaged  
Nusselt number for rising  
bubbles at  $Re^{(2)} = 200$



**Figure 10.**  
Time history of averaged  
Sherwood number for  
rising bubbles at  
 $Re^{(2)} = 200$



#### 4. Concluding remarks

A calculating procedure for time-dependent conjugate heat and fluid flows inside and around a rising single bubble has been developed by combining our previously developed moving mesh method for flows in time-dependent geometries with the zoned algorithm for conjugate viscous flows in steady bubbles. In order to highlight the high fidelity performance of the procedure and reduce the complexity of the problem, the numerical procedure is temporally presented in an axisymmetric formula although it can be easily be expanded to a three-dimensional form. A moving boundary-fitted mesh system is employed to track the deformable gas-liquid interface while conjugate flows in both gas and liquid sides are calculated by a two-block zoned method. The interfacial stresses are employed to calculate the velocity value and to decide the time-dependent bubble shape simultaneously. Governing equations for the rising velocity and acceleration of the bubble are derived according to the forces acting on the bubble. Calculations show that the numerical results of bubble shape at terminal states agree very well with the experiments while time-dependent rising velocity collapse with the asymptotic model based on experimental data. Based on the validations, the algorithm is further employed to study time-dependent dynamics of

---

rising bubbles in a hot water and some preliminary insights of conjugate heat and fluid flows in rising bubbles are obtained. The algorithm can be employed for further analysing heat, mass and momentum transfer phenomena and their relevant mechanisms.

## References

- Bunner, B. and Tryggvason, G. (1998), "Direct numerical simulation of large three-dimensional bubble systems", ASME FEDSM98-5214.
- Dandy, D. and Leal, L.G. (1989), "Buoyancy-driven motion of a deformable drop through a quiescent liquid at intermediate Reynolds numbers", *Journal of Fluid Mechanics*, Vol. 208, pp. 161-92.
- Davidson, M.R. and Rudman, M. (2002), "Volume-of-fluid calculation of heat or mass transfer across deforming interfaces in two-fluid flow", *Numerical Heat Transfer, Part B*, Vol. 41, pp. 291-308.
- Hirt, C.W. and Nichols, B.D. (1981), "Volume of fluid (VOF) method for the dynamics of free boundaries", *Journal of Computational Physics*, Vol. 39, pp. 201-25.
- Hirt, C.W., Amsden, A.A. and Cook, J.L. (1974), "An arbitrary Lagrangian-Eulerian computing method for all flow speeds", *Journal of Computational Physics*, Vol. 14, pp. 227-53.
- Kan, H.C., Udaykumar, H.S., Shyy, W. and Roger, T. (1996), "Simulation of multiphase dynamics by a mixed Eulerian-Lagrangian approach", ASME Paper 96-WA/HT-32.
- Krishna, R. and Baten, J.M. (1999), "Rise characteristics of gas bubbles in a 2D rectangular column: VOF simulations vs experiments", *International Communications in Heat and Mass Transfer*, Vol. 26 No. 7, pp. 965-74.
- Lai, H. and Yan, Y.Y. (2001), "The effect of choosing dependent variables and cell-face velocities on convergence of the SIMPLE algorithm using non-orthogonal grids", *International Journal of Numerical Methods for Heat & Fluid Flow*, Vol. 11 No. 5, pp. 524-46.
- Lai, H., Yan, Y.Y. and Gentle, C.R. (2003), "Calculation procedure for conjugate steady viscous flows about and inside deformable single bubbles", *Numerical Heat Transfer, Part B*, Vol. 43 No. 3, pp. 241-65.
- Lai, H., Yan, Y.Y. and Smith, J.A. (2002), "Calculation procedure with multi-block iteration and moving mesh for heat and fluid flows in complex time-dependent geometries", *International Journal of Numerical Methods for Heat & Fluid Flow*, Vol. 12 No. 2, pp. 106-25.
- Lai, H., Zhang, H. and Yan, Y.Y. (2004), "Numerical study of heat and mass transfer in rising inert bubbles using conjugate flow model", *Numerical Heat Transfer, Part A*, Vol. 46 No. 1, pp. 79-98.
- Mei, R., Klausner, J.F. and Lawrence, J. (1994), "A note on the history force on a spherical bubble at finite Reynolds number", *Physics of Fluids*, Vol. 6 No. 1, pp. 418-20.
- Osher, S. and Sethian, J.A. (1988), "Fronts propagating with curvature dependent speed: algorithm based on Halmilton-Jacobi formulations", *Journal of Computational Physics*, Vol. 79, pp. 12-49.
- Patankar, S.V. (1980), *Numerical Heat Transfer and Fluid Flow*, Hemisphere Publishing Corporation, Washington, DC.
- Raymond, F. and Rossant, J.M. (2000), "A numerical and experimental study of the terminal velocity and shape of bubbles in viscous liquids", *Chemical Engineering Science*, Vol. 55, pp. 943-55.
- Ryskin, G. and Leal, L.G. (1984a), "Numerical solution of free-boundary problems in fluid mechanics. Part 1: the finite-difference technique", *Journal of Fluid Mechanics*, Vol. 148, pp. 1-17.

- Ryskin, G. and Leal, L.G. (1984b), "Numerical solution of free-boundary problems in fluid mechanics. Part 2: buoyancy-driven motion of a gas bubble through a quiescent liquid", *Journal of Fluid Mechanics*, Vol. 148, pp. 19-35.
- Sagaut, P. and Grohens, R. (1999), "Discrete filters for large eddy simulation", *International Journal for Numerical Methods in Fluids*, Vol. 31, pp. 1195-220.
- Salvador, Y. (1994), "Contribution to numerical simulation of flow around a deformable bubble", PhD thesis, ECN-Université de Nantes, Nantes.
- Sato, T., Jung, R.T. and Abe, S. (2000), "Direct simulation of droplet flow with mass transfer at interface", *ASME Journal of Fluids Engineering*, Vol. 122, pp. 510-7.
- Shyy, W., Udaykumar, H.S., Rao, M.M. and Smith, R.W. (1996), *Computational Fluid Dynamics with Moving Boundaries*, Taylor & Francis, Basingstoke.
- Son, G. (2001), "A numerical method for bubble motion with phase change", *Numerical Heat Transfer, Part B*, Vol. 39, pp. 509-23.
- Son, G. (2005), "A level set method for incompressible two-fluid flows with immersed solid boundaries", *Numerical Heat Transfer, Part B*, Vol. 47, pp. 473-89.
- Son, G., Dhir, V.K. and Ramanujapu, N. (1999), "Dynamics and heat transfer associated with a single bubble during nucleate boiling on a horizontal surface", *ASME Journal of Heat Transfer*, Vol. 121 No. 3, pp. 623-31.
- Sussman, M., Smereka, P. and Osher, S. (1994), "A level set approach for computing solutions to incompressible two-phase flow", *Journal of Computational Physics*, Vol. 114, pp. 146-59.
- Thomas, P.D. and Lombard, C.K. (1979), "Geometric conservation law and its application to flow computations on moving grids", *AIAA Journal*, Vol. 17, pp. 1030-7.
- Thompson, J.F., Thames, F.C. and Mastin, C.W. (1974), "Automatic numerical generation of body-fitted curvilinear coordinate system for field containing any number of arbitrary two-dimensional bodies", *Journal of Computational Physics*, Vol. 15, pp. 299-319.
- Trulio, J.G. and Trigger, K.R. (1961), "Numerical solution of the one-dimensional hydrodynamic equations in an arbitrary time-dependent coordinate system", Report UCLR-6522, Lawrence Radiation Laboratory, University of California, Berkeley, CA.
- Tryggvason, G., Bunner, B., Goz, M.F. and Sommerfeld, M. (2001), "Direct numerical simulations of multiphase flows", in Geurts, B.J., Friedrich, R. and Metais, O. (Eds), *In Direct and Large-Eddy Simulation IV*, Kluwer Academic Publishers, Dordrecht, pp. 517-26.
- Univerdi, S.O. and Tryggvason, G. (1992), "A front-tracking method for viscous, incompressible, multi-fluid flows", *Journal of Computational Physics*, Vol. 100, pp. 25-37.
- Van Leer, B. (1979), "Towards the ultimate conservative difference scheme V. A second order sequel to Godunov's method", *Journal of Computational Physics*, Vol. 32, pp. 101-36.

#### Further reading

- Khosla, P.K. and Rubin, S.G. (1974), "A diagonal dominant second-order accurate implicit scheme", *Computers & Fluids*, Vol. 2, pp. 207-9.

#### Corresponding author

Huanxin Lai can be contacted at: [laihuanxin@hotmail.com](mailto:laihuanxin@hotmail.com)